JOURNAL OF GEOPHYSICAL RESEARCH, VOL. 106, NO. B9, PAGES 19,319–19,337, SEPTEMBER 10, 2001

Frictional restrengthening in simulated fault gouge: Effect of shear load perturbations

Stephen L. Karner[1] and Chris Marone[2]

Department of Earth, Atmospheric, and Planetary Sciences, Massachusetts Institute of Technology, Cambridge, Massachusetts, USA

Abstract. Laboratory friction experiments are important for understanding fault restrengthening (healing) between failure events. To date, studies have focused mainly on time and velocity dependence of friction for small perturbations about conditions for steady state sliding. To investigate healing under a wider range of conditions, as appropriate for the interseismic period and dynamic rupture on seismogenic faults, we vary shear load for holds τ_{hold}, hold time t_h, load point velocity V, and initial gouge layer thickness T_0. We shear layers of granular quartz in a biaxial testing apparatus at room temperature and humidity. In addition to conventional slide-hold-slide (CSHS) healing tests, we perform tests in which shear stress is rapidly reduced prior to each hold. Identical slip histories are used in all experiments. Our CSHS tests show time-dependent healing, where $\Delta\mu$ is the difference between peak static friction and prehold sliding friction, consistent with previous work. For a given t_h we find a systematic increase in peak static strength and $\Delta\mu$ with decreasing τ_{hold} (for t_h = 100 s, $\Delta\mu$ = 0.007 for CSHS tests and 0.05 for τ_{hold} = 0 tests). Significantly, healing tests at zero shear stress show decreasing static frictional yield strength with increasing t_h; thus we observe time-dependent weakening in this case. We vary initial layer thickness (0.5-3 mm) and find greater healing for thicker layers. Numerical simulations using rate and state friction laws show that neither the Dieterich nor Ruina evolution laws predict our experimentally observed healing rates for the full range of conditions studied. Our results have significant implications for the mechanics of deformation within granular media. We present a micromechanical model based on stress chains, jamming, and time-dependent unjamming of sheared granular layers. As applied to earthquakes, our data indicate that coseismic stress drop is expected to have an important effect on fault healing rates and static yield strength.

1. Introduction

Investigations of rupture processes that operate during instability and the processes leading to restrengthening of shear zones are key for understanding fault deformation during the earthquake cycle. Considerable effort has been devoted to incorporating these processes into friction constitutive laws that can be applied to faulting [e.g., *Dieterich*, 1979; *Ruina*, 1983; *Chester and Higgs*, 1992; *Perrin et al.*, 1995; *Segall and Rice*, 1995; *Sleep*, 1995; *Marone*, 1998a]. Of these laws the laboratory-derived slip rate and state variable formulations have received the most attention [see *Marone*, 1998b]. Rate and state friction laws describe second-order variations of frictional strength in terms of slip, loading rate, and the state of the shearing zone. Previous laboratory studies have focused on the effect of small deviations from steady state sliding [e.g., *Dieterich*, 1972, 1978; *Lockner et al.*, 1986; *Marone et al.*, 1990; *Blanpied et al.*, 1991; *Chester and Higgs*, 1992; *Fredrich and Evans*, 1992; *Beeler et al.*, 1994; *Karner et al.*, 1997; *Marone*, 1998a]. However, stress variations in the spatiotemporal vicinity of earthquake rupture may be large and complex. Thus a key issue for laboratory studies of rock friction is that of investigating a wider range of conditions, including finite perturbations from steady sliding.

Several recent studies have involved novel experiments designed to understand shear along multicontact interfaces and within granular material [e.g., *Heslot et al.*, 1994; *Nasuno et al.*, 1997, 1998; *Baumberger et al.*, 1999; *Berthoud et al.*, 1999; *Géminard et al.*, 1999]. In rock mechanics, recent studies have concentrated on the frictional effects associated with variations in normal load [*Linker and Dieterich*, 1992; *Richardson and Marone*, 1999], shear load [*Nakatani and Mochizuki*, 1996; *Nakatani*, 1998; *Karner and Marone*, 1998; *Olsen et al.*, 1998], and fast loading velocities [*Mair and Marone*, 1999]. Results from these studies indicate that friction of geologic materials is more complicated than suggested by studies of velocity stepping and slide-hold-slide tests. Moreover, data from studies involving large perturbations in normal or shear load cannot be completely described by the existing friction laws [*Karner and Marone*, 1998].

To further distinguish between the friction laws and to extend the range of conditions studied, we have performed experiments on simulated fault gouge involving large perturbations of shear load. We employed a modified form of the slide-hold-slide (SHS) technique useful for studies of frictional restrengthening (healing). In our tests, shear load was rapidly changed from the prehold sliding level τ_{slide} to a reduced level for holds τ_{hold}. We study healing as a function of shear load (τ_{hold}/τ_{slide} varied from 0 to 1), hold time (1-10000 s), loading rate (10-300 μm/s), and initial gouge layer thickness (0.5-3 mm).

[1] Now at Department of Geology and Geophysics, Center for Tectonophysics, Texas A&M University, College Station, Texas, USA.

[2] Now at Department of Geosciences, Pennsylvania State University, University Park, Pennsylvania, USA.

Paper number 2001JB000263
0148-00227/01/2001JB000263$09.00

Our data show systematic variations in healing and healing rates as a function of these variables. We analyze our data using the time- (Dieterich) and slip- (Ruina) dependent friction laws. Our data are not well described by these laws, indicating that state evolution within fault gouge may depend on parameters other than loading rate and a critical slip distance (e.g., porosity, extent of consolidation, grain size, particle size distribution). To explain our observations, we adopt a model in which the mechanical behavior of fault gouge is effected by the generation and destruction of load-bearing particle chains.

2. Experiment Details

2.1. Testing Apparatus and Sample Description

Our experiments were conducted in a double-direct shear deformation apparatus (Figure 1) at room temperature and room humidity conditions. The apparatus consists of two separate hydraulic loading frames that directly apply normal and shear loads to the sample by using electronic servocontrolled feedback systems. Samples were sheared under load point displacement control with 0.1 μm resolution. Throughout each test, normal force was maintained constant with a control resolution better than 0.1 kN. Loading forces and displacements were monitored at the load point position, and data were sampled at rates up to 10 kHz. For some experiments, we directly monitored gouge layer slip and thickness variations using displacement transducers mounted on the sides of the sample.

For our testing equipment, force measurements and displacements reflect both sample deformation and elastic interaction with the apparatus and forcing blocks (either steel or Westerly granite). To separate these effects, we correct for elastic distortions of the loading frames and sample assemblage. We performed detailed calibrations to determine the elastic properties of the testing apparatus and sample forcing blocks. For the conditions of our tests, the apparatus stiffness in the normal direction is 0.33 kN/μm, and for the shear direction it is 0.50 kN/μm. The forcing blocks have been characterized to account for Poisson distortion during the imposed loading variations (for steel $E = 293$ GPa, $\nu = 0.25$ and for granite $E = 76$ GPa, $\nu = 0.27$).

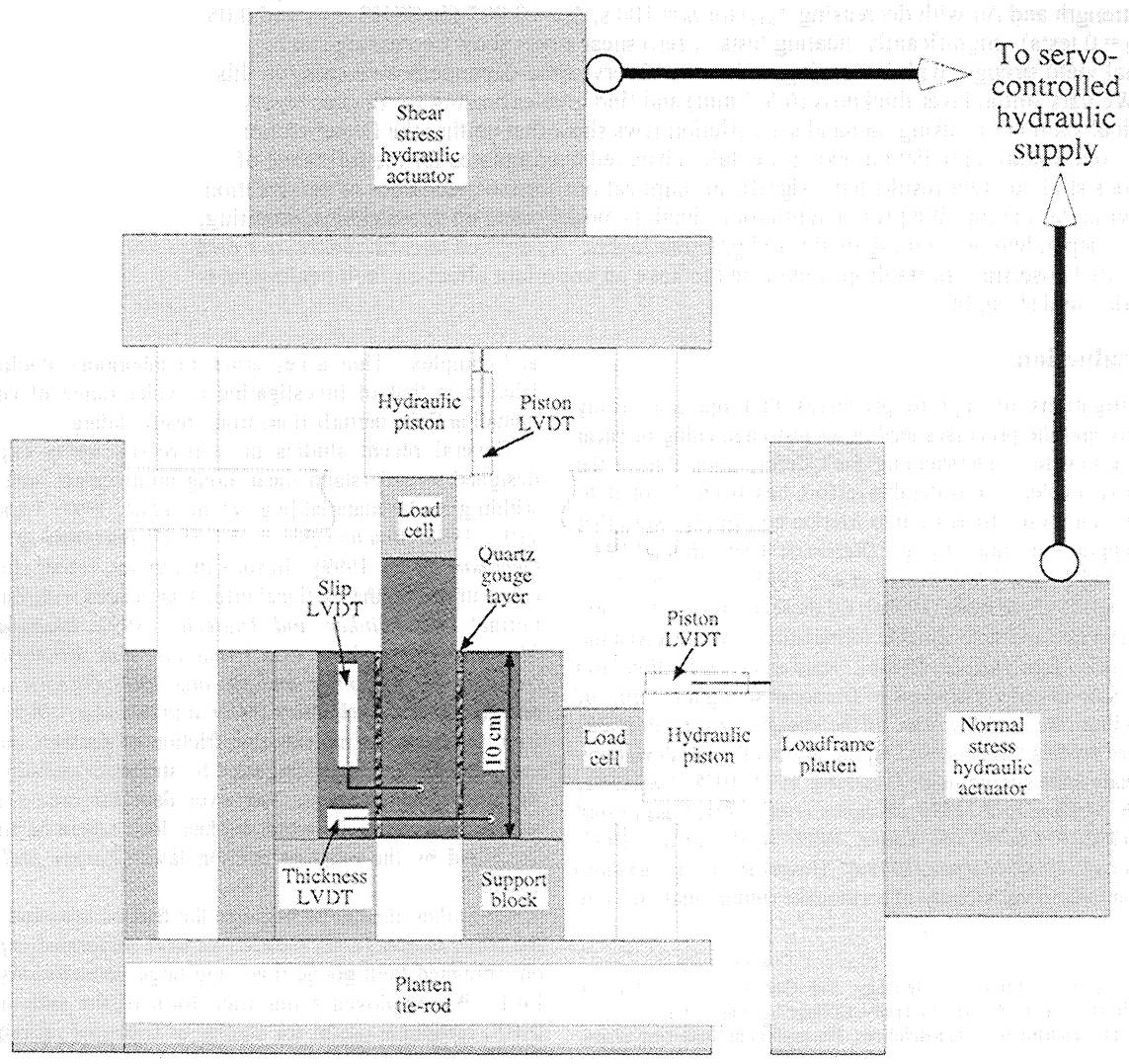

Figure 1. Schematic illustration of the double-direct shear testing apparatus. Two independently controlled loading pistons provide normal and shear stresses. Quartz gouge layers are sheared between solid forcing blocks. Outer blocks are supported from beneath and the central block is driven between them. Displacement transducers mounted on the sample measure fault slip and layer thickness directly.

Samples consisted of gouge layers sandwiched between forcing blocks arranged in a triple block geometry (Figure 1). Gouge layers were composed of granular quartz obtained from the US Silica Company (trade name F-110). The quartz particles are initially subangular and have initial grain size of 50-150 μm (110 μm RMS) (see *Mair and Marone* [1999] for a description of this material). The nominal contact area is 10x10 cm^2. Central forcing blocks are longer in the shear direction so that up to 5 cm of slip can be achieved.

For our sample geometry, slip is accommodated within both gouge layers. To eliminate boundary shear and to force shear to occur within the layers, we machine evenly spaced grooves on the shear surfaces of the steel forcing blocks, and the granite forcing blocks were roughened by sandblasting with a 60-grit abrasive. To minimize gouge loss along the unconfined lateral edges of the layers, we attach lubricated plates to the stationary side blocks of each sample. Thin copper shims beneath the side blocks and gouge layers further minimize gouge loss. To reduce apparatus friction we grease all moving and mated parts with a molybdenum disulfide lubricant.

2.2. Experiment Procedure

2.2.1 Conventional slide-hold-slide tests. Previous laboratory studies have employed slide-hold-slide tests to investigate frictional restrengthening [e.g., *Dieterich*, 1972, 1978; *Chester and Higgs*, 1992; *Beeler et al.*, 1994; *Karner et al.*, 1997; *Marone*, 1998a]. We also performed conventional slide-hold-slide (CSHS) tests. We sheared quartz gouge layers (initially 3 mm thick) at a rate of 10 μm/s, and maintained normal stress constant (25 MPa). Measurements of layer thickness, slip across a layer, and the calculated frictional response for a typical test are shown in Figure 2. During a hold, friction decays owing to sample creep and elastic interaction with the loading apparatus (Figure 2a). The frictional relaxation during holds is accompanied by compaction of the gouge layer (Figure 2b). When loading is resumed, gouge layers dilate and friction increases to a maximum value corresponding to the traditional

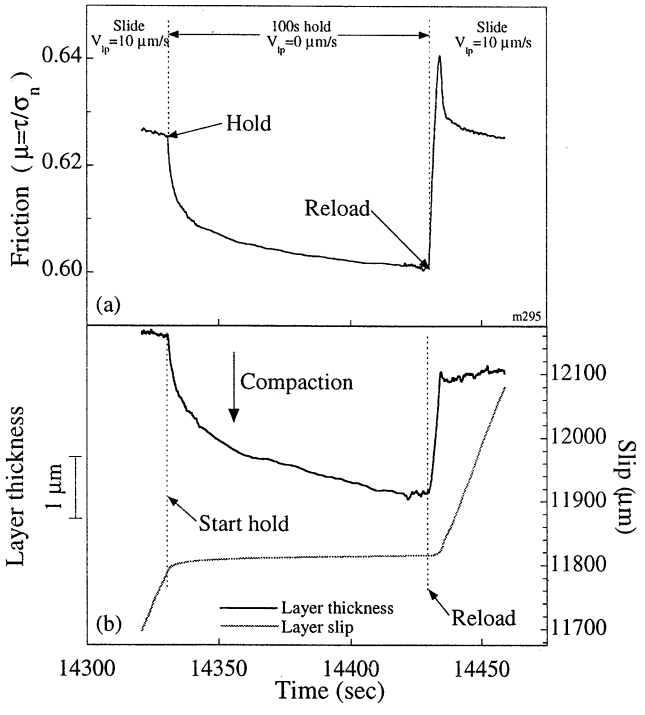

Figure 2. Data from a conventional slide-hold-slide (CSHS) test. In these experiments, samples are sheared at a given load point velocity followed by "holds" initiated by setting the loading velocity to zero. (a) At the onset of a hold, friction decays from the steady state sliding level. On reload, friction increases to a maximum value (static friction) before returning to its initial level. Healing is defined as the difference between reload static friction and prehold sliding friction. (b) Layer thickness and slip as measured across a gouge layer, for the same hold shown in Figure 2a. At steady-state, slip rate equals the imposed loading velocity. During holds, layer slip continues and the rate of slip decays with time. Layers compact during holds. On reload, layers dilate and slip rate increases.

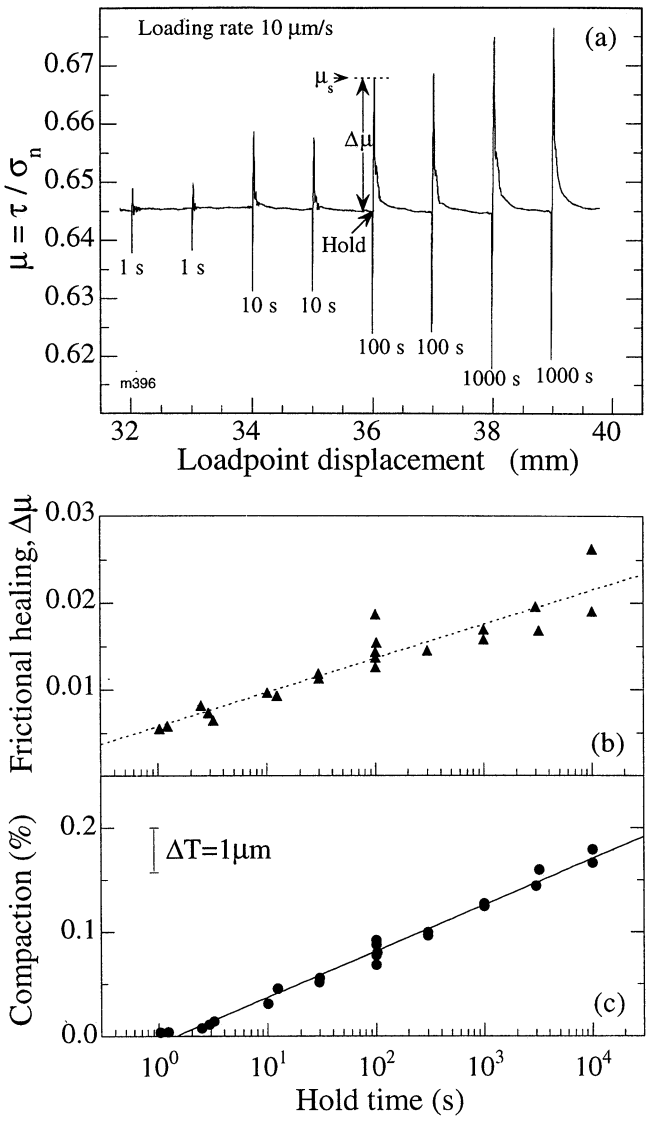

Figure 3. Data from CSHS tests. (a) Friction data are plotted against load point displacement. During a hold, load point position is held constant. We measure healing Δμ as the difference between prehold sliding friction and reload static friction μ_s. (b) Healing data are shown for loading velocity of 10 μm/s. Data indicate that Δμ increases linearly with log hold time. (c) Hold compaction for one gouge layer is plotted against hold time. Change in porosity is calculated from the measured layer thickness variation ΔT and nominal contact area, normalized by the initial gouge layer volume. Data show that compaction proceeds linearly with log hold time.

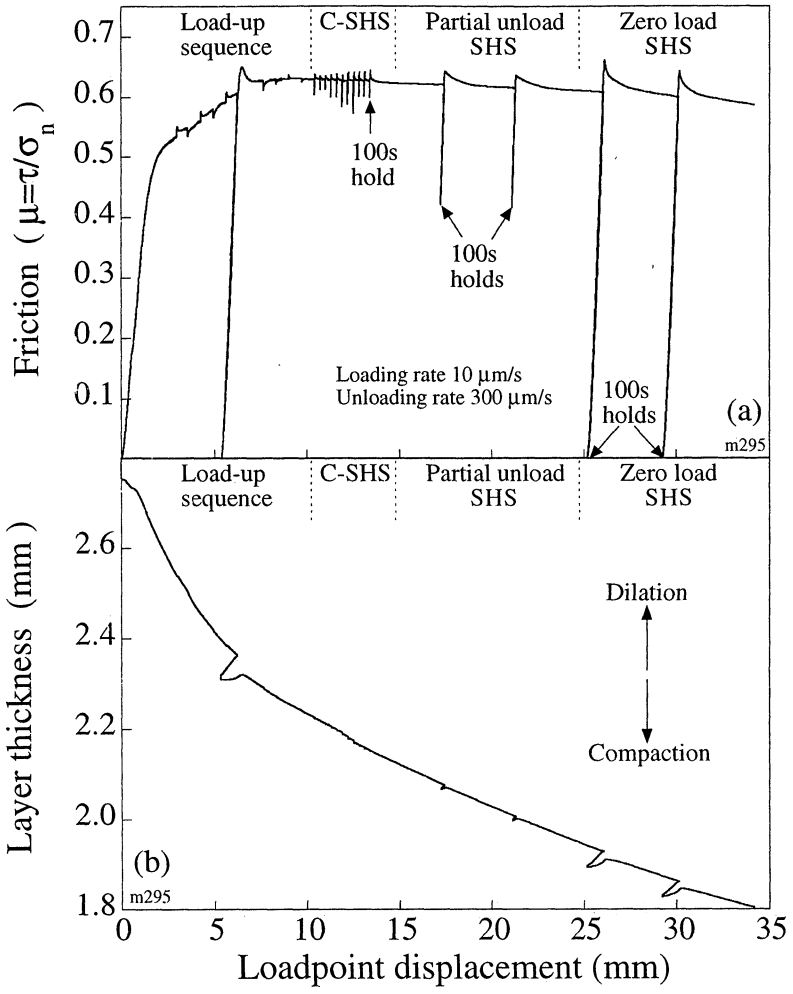

Figure 4. Data from one experiment involving holds at different shear loads. (a) Friction is the ratio of measured shear and normal stress and is plotted against load point displacement. Base level sliding friction decreases slightly with slip. Data show a set of CSHS tests with hold times of 10, 100, 1000, and 10000 s. The last three hold cycles of the series were of 100 s duration. For comparison, the next two hold cycles (100 s) were performed at a reduced shear load ($\mu_{hold} \sim 0.4$), and the last two hold cycles involved complete removal of shear load. Peak static yield strength increases as τ_{hold} decreases. (b) Layer thickness data are shown for the same experiment shown in Figure 4a. Layers thin with increasing shear displacement. Layer thickness variations are larger for holds with lower levels of τ_{hold}.

definition of "static" friction. The difference between static friction and prehold sliding friction is taken as a measure of restrengthening ($\Delta\mu$, which we refer to as healing).

Healing and layer thickness data for a series of CSHS tests are shown in Figure 3. For simulated fault gouge, $\Delta\mu$ increases with hold time and is in the range 0.005-0.015 for times (t_h) of 1-100 s (e.g., Figures 3a and 3b). Healing rates, $\beta = \Delta\mu/\Delta\log_{10} t_h$, are typically between 0.003 and 0.02 (e.g., Figure 3b). Layer compaction for holds is also observed to increase with $\log_{10} t_h$ (e.g., Figure 3c). Gouge layer thinning, coupled with continued sample creep during holds, indicates that shear enhanced compaction may be a key mechanism responsible for healing and time-dependent restrengthening of fault gouge. However, healing in these tests involves both time- and slip-dependent processes, making it difficult to separate their effects (see *Beeler et al.* [1994] for a novel way to achieve this for CSHS tests). Thus it is important to design laboratory experiments to isolate the effects of time and slip.

2.2.2. Reduced load slide-hold-slide tests. To investigate time-dependent processes, we performed experiments using a technique similar to that of the CSHS tests described above. Gouge layers were sheared at a reference loading rate that was interrupted for specified periods of time (holds). Our experiments differ from CSHS tests in that shear load was rapidly reduced prior to initiating holds [e.g., *Nakatani and Mochizuki*, 1996; *Karner and Marone*, 1998; *Nakatani*, 1998; *Olsen et al.*, 1998](see Figures 4-6). In this way, shear creep of the sample is limited or does not occur at all during holds. Shear load was decreased by retracting the loading piston at a fast rate (up to 300 μm/s) using displacement feedback servocontrol, together with a comparator circuit to stop unloading at a preset shear stress level. Complete removal of shear load occurred within 2.5-3 s for the stiffness, loading conditions, and sample dimensions of our tests. Holds were timed from the point when the reduced shear load (τ_{hold}) was reached, to the time that reloading began.

Data from numerous trial experiments indicated that the frictional response following hold cycles was strongly dependent on sample slip history. Thus the data reported here were obtained from experiments with identical slip histories, including the initial loading sequence to ~10 mm displacement (as seen in

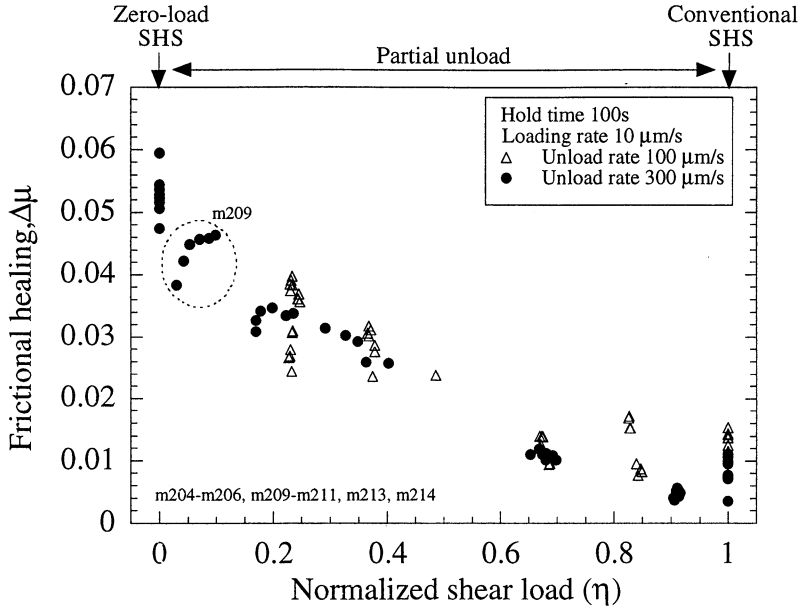

Figure 5. Healing is shown as a function of shear stress during the hold, $\eta = \tau_{hold}/\tau_{ss,prehold}$. Data show that healing increases as η decreases and that unloading rate has a negligible effect. Data scatter shows experiment reproducibility, and for a given experiment (e.g., "m209" where $0.030 < \eta < 0.098$), scatter is due to the decrease in the coefficient of sliding friction with displacement (e.g., Figure 4a).

Figure 4). Velocity steps in the loading sequence allow for determination of the friction parameters (a, b, and D_c) prior to holds, while the loading cycle serves to condition the gouge layers and sample assembly. Following the loading sequence, hold cycles were implemented at regulated slip intervals. Holds were imposed as consecutive pairs, and three sets of hold pairs were typically performed within the shear displacement possible for our samples. Identical hold times were used for the first and last hold pairs, and we varied the hold time for the middle set. Table 1 summarizes details of the experiments.

3. Results

3.1. The Effects of τ_{hold}

For direct comparison to data from CSHS tests (e.g., Figures 2 and 3) we conducted SHS tests on layers of quartz gouge and varied the shear load for holds τ_{hold}. To address differences in base level sliding friction between each experiment, we normalize τ_{hold} by the measured prehold shear stress value τ_{slide} and define this dimensionless ratio as η. Thus for CSHS tests, η equals unity, and for zero-load SHS the ratio is 0. Our data show distinct and systematic variations as a function of η.

3.1.1. Frictional restrengthening. In Figure 4 we show data from a single experiment in which holds were conducted at different levels of shear stress. Three consecutive pairs of 100 s holds are shown for which η was systematically decreased from 1 to 0. The general features of the reduced load SHS data are similar to those of CSHS tests (compare Figure 4 with Figures 2-3). That is, static friction is greater than the prehold sliding levels. To remain consistent with previous studies, we quantify healing $\Delta\mu$ as the difference between static friction and the prehold sliding value (e.g., Figure 3). For a given hold time, the data in Figure 4a show lower $\Delta\mu$ for holds at larger values of η, and that the dependence of healing on η is significant. On reloading after holds at lower η, more slip is required to return friction to the prehold "steady state" sliding level.

We investigated the systematic relationship between $\Delta\mu$ and η (Figure 5). These data are consistent with results from individual experiments (e.g., Figure 4a) in that healing decreases as η increases from 0 to 1. Furthermore, the data show that healing is significantly dependent on η inasmuch as healing for zero-load SHS tests is 5-10 times greater than that for CSHS tests ($\Delta\mu \sim 0.047$-0.06 for $\eta = 0$, and $\Delta\mu \sim 0.003$-0.01 for $\eta = 1$). For 100 s holds our data indicate that healing $\Delta\mu$ is lowest when $\eta \sim 0.9$. The occurrence of this minimum is consistent with previous observations that sample creep is significantly reduced when shear load falls below 90% of the sliding friction level [*Olsen et al.*, 1998].

3.1.2. Layer thickness variations. Hold cycles conducted at larger η result in smaller perturbations in layer thickness (Figure 4b). This is particularly evident when data for individual hold cycles are viewed in detail. Figure 6 shows data from two 100 s holds, one in which shear load was partially reduced and one with $\tau_{hold} = 0$. Changes in layer thickness scale with the magnitude of shear stress reduction prior to a hold. We distinguish three components of thickness corresponding to the unloading, the hold, and the reload portions of the hold cycles (Figure 6b). For unloads we observe significant layer compaction, which continues through the holds. Layers dilate during reloading. The amount of unload compaction ΔT_u, and reload dilatancy ΔT_r, decreases for larger values of η (note the different layer thickness scale for Figures 6b and 6d). Furthermore, for a given hold cycle, ΔT_u is greater than ΔT_r; hence holds result in net compaction of the entire layer.

To compare with healing data for all 100 s holds (Figures 5 and 7a), we show layer thickness variations for the unload, hold, and reload portions for these hold cycles (Figures 7b-7d). For clarity, we plot mean values of healing, change in layer thickness, and η, with ± 1 standard deviation about the mean. Unload

compaction decreases systematically as η increases (Figure 7b). We observe little (or no) η dependence on compaction during holds and a systematic decrease in reload dilatancy for greater levels of η. For a given η, data scatter (indicated by the error bars) arises from experiment reproducibility and from the slip-dependent layer compaction (e.g., Figures 4 and 5).

3.1.3. Layer slip during hold cycles. Our direct measurements on the sample assembly show that gouge layers experience some reverse slip as η approaches zero, typically of the order of 1-10 μm (Figure 6d, see inset for more detailed view of measured slip). This is surprising because the loading piston is not rigidly connected to the center forcing block and hence cannot physically reverse the slip direction. We attribute slip reversal to compaction and time-dependent decay of elastic strain within the gouge layers. We also considered the possibility of time-dependent distortion of the forcing blocks. However, detailed measurements of apparatus and sample distortion show that such effects must be minor, as slip reversals are not observed for intermediate levels of η. We expect that slip reversals have a small effect on the resulting healing behavior. As these observations are novel, systematic, and reproducible, we shall return to them later to briefly discuss their origins and the implications for deformation in granular media.

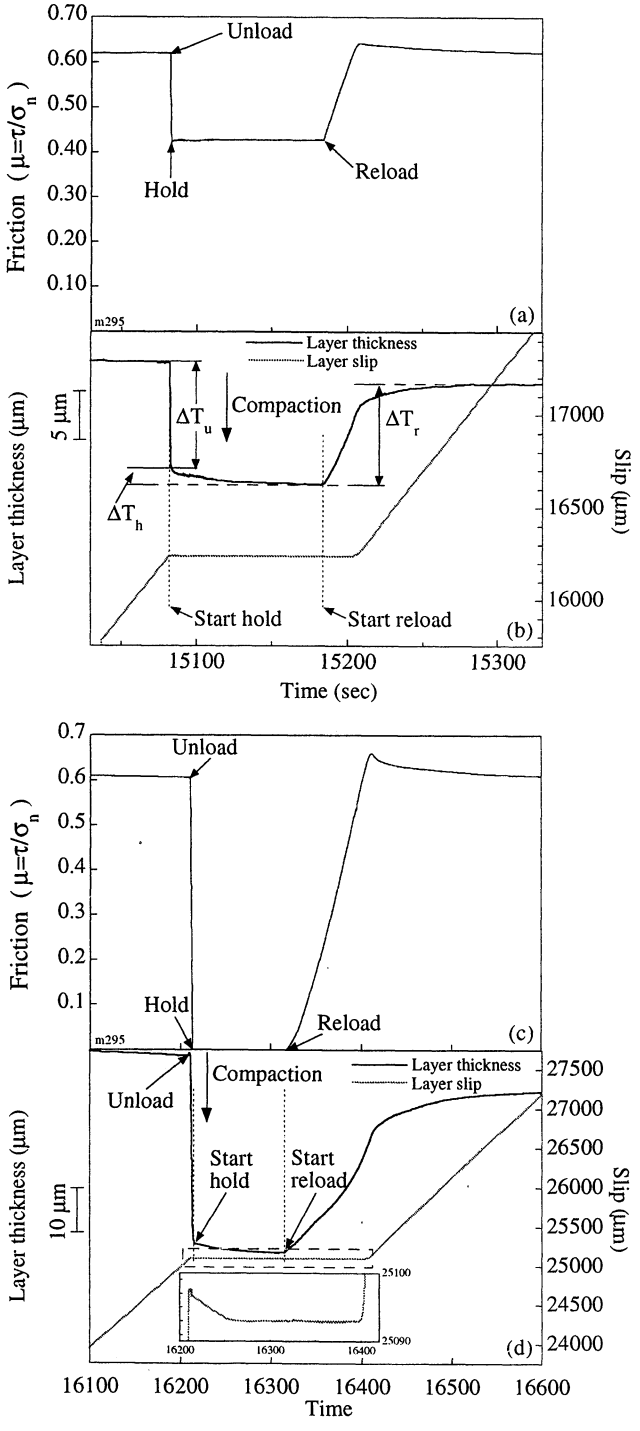

Figure 6. Data for reduced-load SHS tests. (a) Friction data are shown for the partial-load SHS test of Figure 4. Unloading from steady state sliding is 300 μm/s, and holds are timed from the point at which τ_{hold} is reached to the point of reloading. Friction is nearly constant during holds, indicating negligible creep slip. Healing is defined in the same way as CSHS tests. (b) Layer thickness and slip measurements from the sample mounted displacement transducers for the same hold shown in Figure 6a. Significant compaction occurs during unloading, and compaction continues into holds. On reload, gouge layers dilate but not enough to recover porosity loss during unloading. For partially stressed holds, sample slip stops soon after unloading begins. (c) Friction data shown for the first zero-load SHS hold in Figure 4. The general features are similar to those of CSHS tests and to partial-load SHS holds. Peak static yield strength on reloading is greater than for stressed SHS tests. (d) Layer thickness and slip measured on the sample are plotted. Unload compaction and reload dilatancy are larger than for partial-load SHS tests. Layers compact during holds. In the inset, note that during unloading and into the hold, sample slip reverses slightly.

3.2. Time-dependence for $\eta = 0$

In Figures 8-10 we show data from experiments designed to investigate the effects of hold time t_h. For reference, we show in Figure 8a the loading curve for a representative experiment where t_h for the middle hold pair differs from those of the other holds. We show the healing data from this experiment in Figure 8b together with healing data from another test involving the same hold times but in reverse order. For a given experiment, Δμ and sliding friction decrease with increased slip. Healing for the third and fourth holds departs systematically from the nearly linear displacement-dependent trend of the other holds. Data for the two 100 s holds from "m165" show lower Δμ compared to the trend defined by the 10 s holds. Conversely, for "m166" the two 10 s holds yield larger Δμ compared to the trend of the other holds. This observation is reproducible, in that our zero-load SHS data consistently show lower Δμ for longer hold times. Furthermore, this observation is independent of hold sequence order. In Figures 8c-8e we show the layer thickness data corresponding to the hold cycles of Figures 8a-8b. The first order observation is that the layer thickness variations are smaller as total displacement increases. However, the data also show that longer hold times result in more gouge compaction (Figure 8d). For both tests, compaction during the 10 s holds is less than compaction measured for 100 s holds.

To compare experiments, we remove the displacement effect using a linear fit to the data from the first and last hold pairs and then reference the values to a displacement of 20 mm. In Figure 9 we show the detrended healing data for all SHS tests where samples were sheared at 300 μm/s. The detrended values are

Table 1: Experiment Summary.

Experiment	Initial Layer Thickness, mm	Loading Rate, μm/s	Normal Stress, MPa	Forcing Block Material	μ for Hold, μ_{hold}/μ_{ss}	Nominal Hold Time, s
			η dependence for 100 s holds			
m295	3	10	25	steel	combination	10-10000
m213	3	10	25	steel	1	100
m214	3	10	25	steel	0.910	100
m211	3	10	25	steel	0.593	100
m206	3	10	25	steel	0.346	100
m210	3	10	25	steel	0.195	100
m209	3	10	25	steel	0.064	100
			Time and η dependence			
m386	3	10	25	steel	1.0	1-10000
m389	3	10	25	steel	0.83	1-3000
m385	3	10	25	steel	0.83	1-10000
m366	3	10	25	steel	0.68	10, 100
m369	3	10	25	steel	0.68	10-1000
m368	3	10	25	steel	0.68	1000, 10000
m365	3	10	25	steel	0.35	1-100
m363	3	10	25	steel	0.35	10-1000
m362	3	10	25	steel	0.35	100, 1000
m364	3	10	25	steel	0.35	1000, 10000
m371	3	10	25	steel	0.25	1, 10
m353	3	10	25	steel	0.25	1-100
m352	3	10	25	steel	0.25	10-1000
m370	3	10	25	steel	0.25	100, 1000
m354	3	10	25	steel	0.25	1000, 10000
m350	3	10	25	steel	0.25	100, 1000
			Time dependence for η=0			
m165	3	300	25	steel	0	10, 100
m166	3	300	25	steel	0	10, 100
m167	3	300	25	steel	0	10, 1000
m168	3	300	25	steel	0	10, 100
m169	3	300	25	steel	0	100, 1000
m170	3	300	25	steel	0	100, 1000
m175	3	300	25	steel	0	1000, 10000
m204	3	10	25	steel	0	100, 1000
m205	3	10	25	steel	0	100, 1000
m207	3	10	25	steel	0	1000, 10000
			Vary initial layer thickness, η=0			
m231	3	10	15	Westerly	0	100, 1000
m235	2	10	15	Westerly	0	10, 100
m232	2	10	15	Westerly	0	100, 1000
m247	2	10	15	Westerly	0	1000, 10000
m236	1	10	15	Westerly	0	10, 100
m248	1	10	15	Westerly	0	10, 100
m233	1	10	15	Westerly	0	100, 1000
m250	1	10	15	Westerly	0	1000, 10000
m246	0.5	10	15	Westerly	0	10, 100
m244	0.5	10	15	Westerly	0	100, 1000
m251	0.5	10	15	Westerly	0	1000, 10000

large compared to CSHS tests, consistent with the inverse η dependence of healing (e.g., Figure 5). Furthermore, we observe negative healing rates (thus, time-dependent weakening) consistent with our observations from a limited data set [*Karner and Marone*, 1998]. This time-dependent weakening contrasts with positive healing rates from CSHS tests (Figure 3b).

In Figures 10a-10d we present data from all zero-load SHS tests where samples were sheared at rates of 10 or 300 μm/s. For clarity, the data are shown as mean values ±1 standard deviation. Both the healing and compaction data have been corrected for displacement effects as outlined above. For each loading rate we observe large healing values. However, static friction levels and Δμ are slightly smaller for the loading rate of 300 μm/s. Healing data from the 300 μm/s tests show time-dependent weakening, while for 10 μm/s we observe little or no time dependence of healing.

Layer thickness data from these same tests show that hold compaction ΔT_h increases with hold time but that time-dependent compaction is smaller than ΔT_u or ΔT_r (Figure 10). ΔT_u is independent of hold time, which is expected as holds are imposed after unloading. ΔT_r is also roughly independent of hold time, indicating that dilatancy is dominated by time-independent elastic processes. Samples loaded at 10 μm/s undergo less compaction during holds than samples loaded at 300 μm/s. Thus faster loading rates result in greater hold compaction and lower healing levels. This correlation is consistent with our observations that time-dependent weakening is associated with greater compaction during holds. We also note that ΔT_r is independent of loading

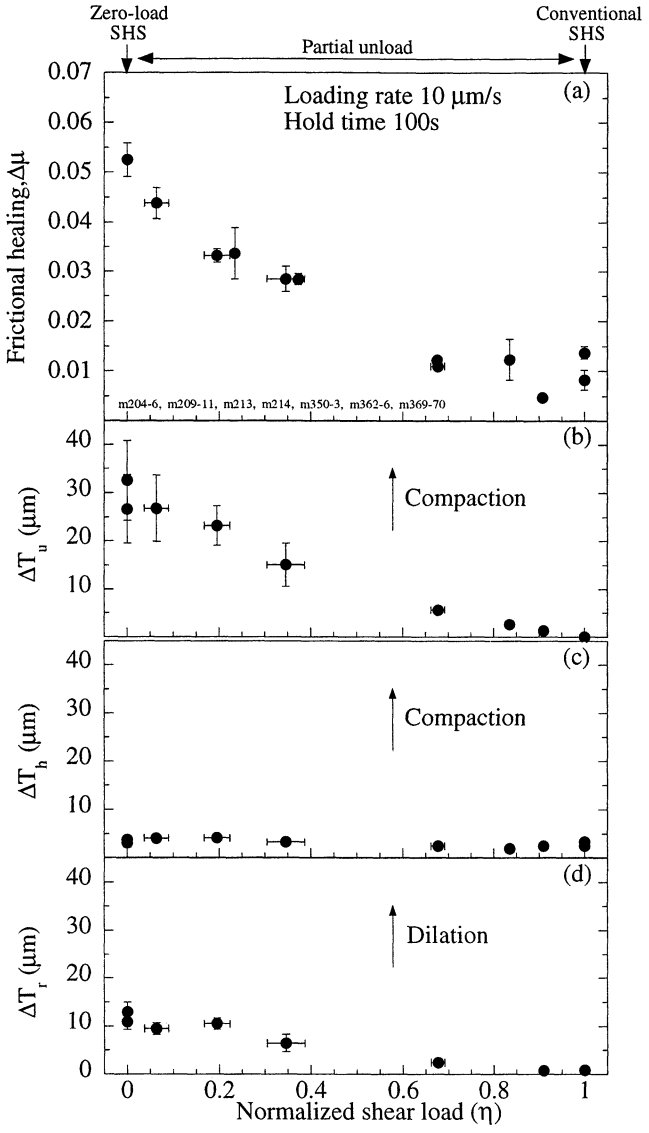

Figure 7. Friction and layer thickness as a function of η. Layer thickness has been corrected for elastic interaction with the testing apparatus and for distortion of the forcing blocks. Data are shown as mean values ±1 standard deviation. (a) Healing data are replotted from Figure 5, showing larger healing levels for lower η. (b) Changes in layer thickness is measured during unloading for the same hold cycles shown in Figure 7a. Layers compact more for lower levels of τ_{hold}. Data scatter for a given η is due to the displacement-dependent thinning (and hence porosity reduction) of the gouge layer. (c) Compaction is measured during 100 s holds. The data show little to no dependence of hold compaction on η. (d) Reload dilatancy is larger for lower levels of η, but dilatancy is less than the total compaction that occurs during the hold cycle prior to reloading.

rate, which indicates that reloading duration does not significantly influence the magnitude of dilatancy.

3.3. Layer Thickness Dependence of Healing

To investigate the effect of gouge layer thinning on healing and sliding friction (Figures 4 and 8), we performed zero-load SHS tests on layers with differing starting thickness (T_0 between 0.5 and 3 mm). For these tests we used rough Westerly Granite forcing blocks. Results are corrected to a shear displacement of 20 mm, as outlined above. For a given hold time, healing increases with thickness (i.e., larger T_0, Figure 11a), a trend that is consistent with the observed displacement dependence on healing (e.g., Figure 8b). Healing data from tests with T_0 of 2 and 3 mm show time-dependent weakening, consistent with our previous observations (e.g., Figures 8-10). Healing values from tests with T_0 of 0.5 and 1 mm are almost identical, and the data show little or no time-dependent weakening.

To illustrate the relationship between healing and layer compaction for different T_0, we present the measured layer thickness changes for unloads, holds, and reloads of 100 s hold cycles in Figures 11b-11d. All data have been corrected for Poisson distortion of the forcing blocks as described above. For a given T_0, unload compaction is significantly larger than compaction during holds and reload dilatancy. Thicker samples experience larger changes in layer thickness which are associated with greater levels of healing. We observe similar trends for other hold times.

4. Discussion

4.1. Comparison With Previous Work

Our conventional slide-hold-slide tests show that layer slip and compaction occur during holds and that healing increases with longer hold times (time-dependent strengthening; Figures 2-3). Healing levels and layer thickness variations decrease with increasing shear stress η (Figures 4-7). Data from tests where η = 0 show large healing levels, which decrease with longer hold times (time-dependent weakening), coupled with positive compaction rates for holds (Figures 8-10). We observe that healing levels, healing rates, and layer thickness variations scale with initial thickness of the gouge layer (Figure 11). Of our results, the more significant observations are (1) that the strength of quartz fault gouge varies significantly with η and (2) that healing rates transition from time-dependent strengthening for η = 1 to time-dependent weakening for η = 0.

It is instructive to compare our results to data from similar experiments designed to determine the effects of holding shear stress on healing. While the existing database is small, the data must be separated into two categories: (1) shear within granular materials [*Karner and Marone*, 1998; *Nakatani*, 1998; *Olsen et al.*, 1998; *Géminard et al.*, 1999; this study] and (2) shear on bare surfaces having many contacting asperities [*Nakatani and Mochizuki*, 1996; *Berthoud et al.*, 1999]. The data indicate significant differences between the two categories, which is consistent with previous research showing that the micromechanical processes associated with sliding on bare surfaces differ from those for shear within simulated fault gouge [e.g., *Byerlee*, 1967; *Scholz*, 1987; *Marone et al.*, 1990; *Beeler et al.*, 1996; *Marone*, 1998b].

4.1.1. Healing behavior in granular media. *Nakatani* [1998] sheared 0.5 mm thick layers of granitic fault gouge in a biaxial apparatus (normal stresses of 5 and 10 MPa) by using shear load as the control parameter, rather than loading velocity as for our experiments. His reduced load SHS data show that healing decreases with greater η, in qualitative agreement with our results (e.g., Figure 5). However, the η dependence that he observed was large compared to our results (Figure 12a). While he did not present supporting data, *Nakatani* [1998] stated that time-dependent strengthening was only observed when η > 0.9 and that healing rates exhibited no significant time dependence for lower η. These comments are consistent with our results from

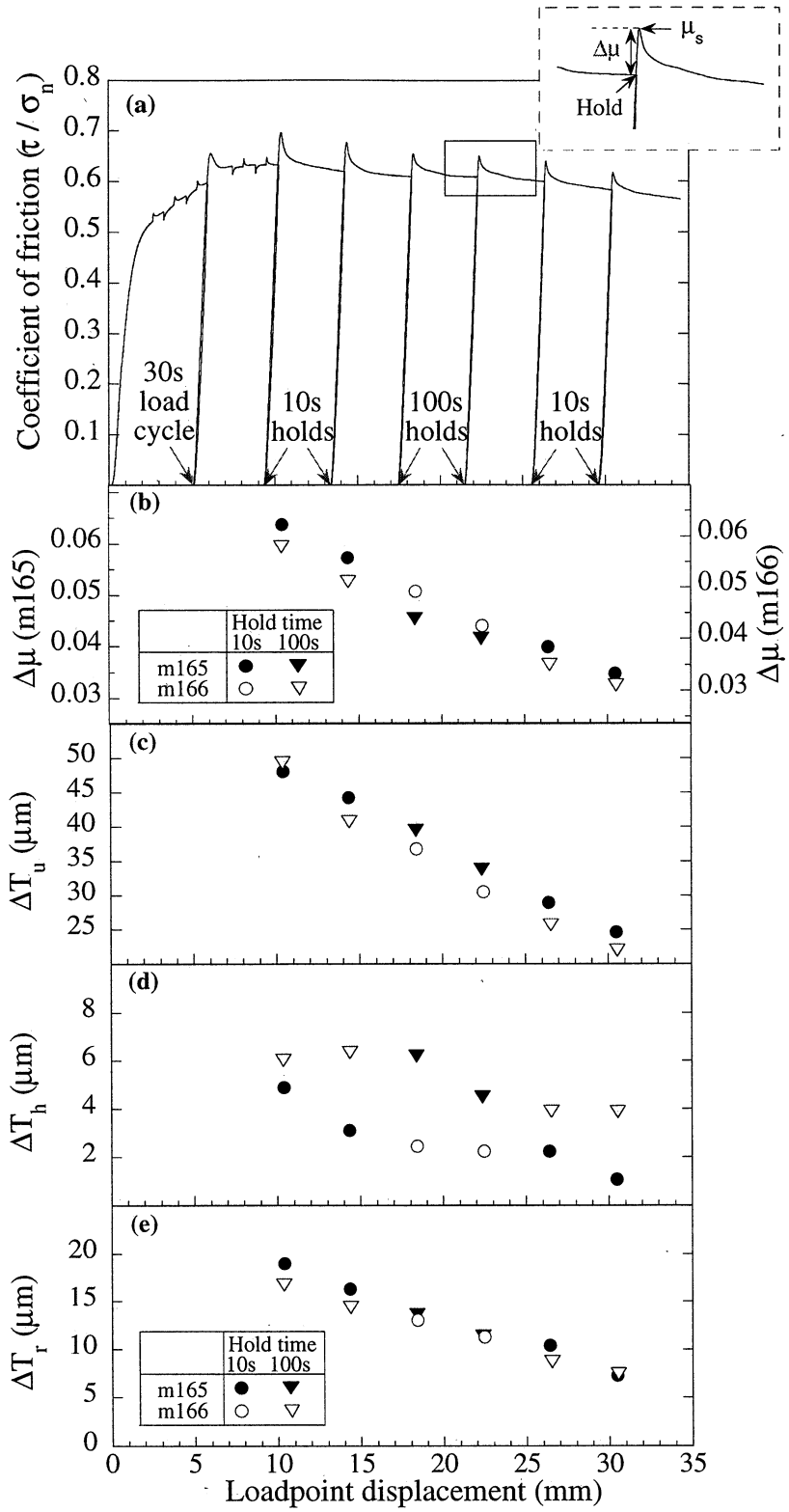

Figure 8. Data from zero-load SHS tests. Layer thickness data are corrected for elastic effects and gouge loss. (a) Friction versus load point displacement is shown for a representative test. All tests were subjected to the exact same loading and displacement sequence. (b) We plot healing data from two tests as a function of displacement. Y-axes are offset to account for differences in base level friction and to allow direct comparison. Data show a strong displacement dependence and that healing is systematically smaller for longer holds. (c) We plot compaction during unloading for the same holds shown in Figure 8b. The displacement dependence of unload compaction is similar for the two tests. (d) Compaction during holds is shown. Longer holds result in greater layer compaction. (e) Layer dilatancy is plotted for the same hold cycles. Data show a displacement-dependent decrease in dilatancy and little dependence on hold time. After *Karner and Marone* [1998].

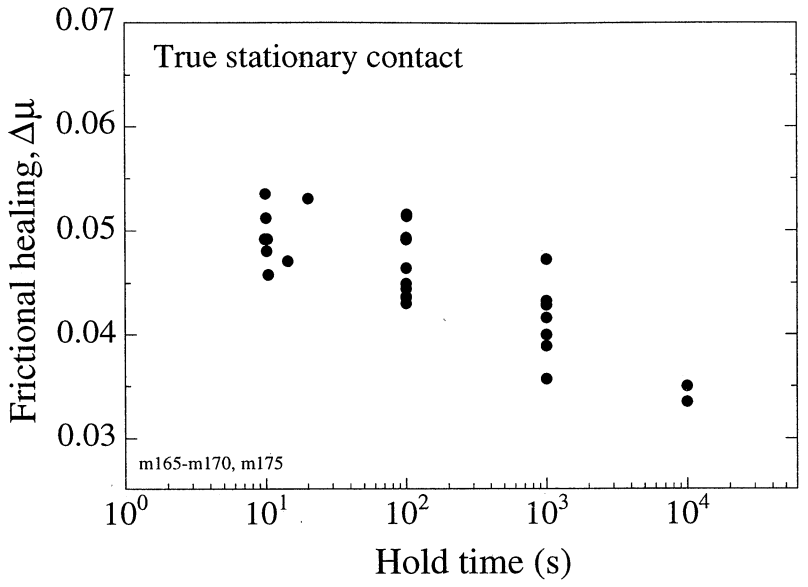

Figure 9. Friction data from all zero-load SHS tests. Healing and peak static yield strength decrease with increasing hold time, indicating time-dependent weakening. Data have been corrected for displacement as described in the text. Data scatter indicates experiment reproducibility. All data are for 3 mm thick layers and 300 μm/s load/unload rate.

conventional and zero-load SHS tests (Figures 3 and 9) and from experiments we conducted at intermediate values of η (discussed further in section 4.4).

Olsen et al. [1998] conducted reduced-load SHS experiments in a triaxial pressure vessel at hydrothermal conditions (P_c = 60 MPa, P_f = 10 MPa, and temperatures of 25°-250° C). Their gouge layers (T_0 = 3.5 mm) consisted of feldspar/quartz granular aggregates with particle sizes between 210 and 500 μm. While it may not be appropriate to directly compare results from their hydrothermal tests to our room temperature experiments, there are features that warrant comment. *Olsen et al.* [1998] imposed hold times that extended to 2 days, and axial load for holds was 40 MPa lower than the steady state sliding level (η = 0.7). They observed healing levels (in terms of shear stress) from ~0.75 to 5.35 MPa, in qualitative agreement with the healing levels from our tests. Their data show no time-dependent strengthening, consistent with observations from our zero-load SHS tests. As the hydrothermal conditions of their tests favor diagenesis, they suggested that the formation of authigenic clays significantly influenced healing and frictional strength.

Géminard et al. [1999] and *Losert et al.* [2000] performed experiments similar to our conventional and zero-load SHS tests. They used a spring slider apparatus to shear layers of fluid-saturated glass beads at room temperature and low normal stress (σ_n = 30-60 Pa). The general features of their data were similar to ours, in that friction after holds increased to a maximum and subsequently decayed to stable sliding levels. For hold times less than 10^4 s, samples loaded from zero shear stress exhibited greater healing than samples loaded from a prestressed state [*Losert et al.*, 2000]. Thus their data indicate lower healing with increasing η, consistent with our observations. Furthermore, their data show positive healing rates for CSHS tests and no time-dependent strengthening for zero-load SHS tests, consistent with the correlation between healing rates and η shown by our data.

***4.1.2.* Healing for shear on bare surfaces.** *Nakatani and Mochizuki* [1996] conducted reduced-load SHS tests on bare granite surfaces at a normal stress of 5 MPa. They presented data for hold times of 30, 300, and 3000 s and for a range of friction levels for holds ($0.842 < \mu_{hold} < 0.016$). In Figure 12a we compare our healing data for 100 s holds to *Nakatani and Mochizuki* [1996] results interpolated for 100 s holds. They observed large healing values (Δμ between 0.03 and 0.13), increased restrengthening for higher levels of μ_{hold} and time-dependent strengthening for all levels of μ_{hold} (e.g., Figure 12b). These results contrast with the inverse η dependence and the lack of time-dependent strengthening we observe.

Similar experiments have also been performed on multicontact interfaces between polymer glasses by *Berthoud et al.* [1999] who used a spring slider track to investigate the effects of shear stress and temperature (25°-125° C) on static friction levels. They performed both conventional- and zero-load SHS tests (their "stressed-aging" and "free-aging" tests, respectively) on nominally flat surfaces of poly-methyl-metacrylate (PMMA) and polystyrene. Their data from stressed-aging tests show large healing levels (Δμ ~0.075-0.85) and positive healing rates (their β_s^r, expressed per decade time) that range from ~0.015 at room temperature to 0.13 for the higher temperatures. They also observe that healing rates for stressed-aging tests are ~2 times greater than the rates observed for free aging, which is in qualitative agreement with observations from bare rock surface experiments [*Nakatani and Mochizuki*, 1996].

These comparisons indicate that the time-dependent weakening we observe and the reduction in healing with increasing η are a granular effect due to particle reorganization processes that do not occur for multicontact surfaces.

4.2. Healing Rates

We also compare our healing rates with those of *Nakatani and Mochizuki* [1996] (Figure 13). We reference our data to 20 mm shear displacement (as outlined above) and show mean values ±1 standard deviation. For a given hold time, healing decreases with

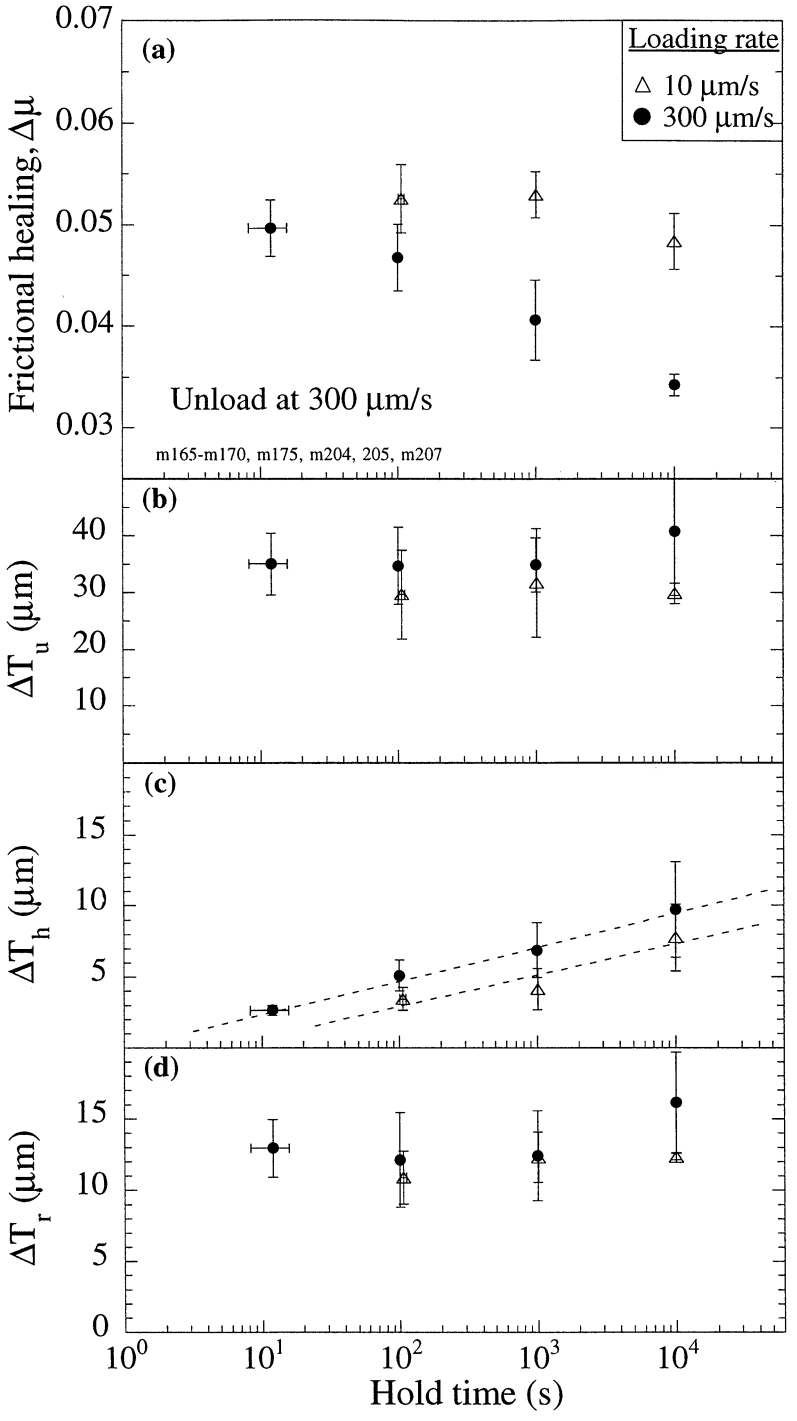

Figure 10. Data from all zero-load SHS tests (gouge layers initially 3 mm thick), plotted as a function of hold time, in terms of mean values with bars indicating standard deviation. Results are shown from tests with two different loading rates (10 μm/s and the 300 μm/s data from Figure 9). Data have been corrected for displacement as described in the text. Layer thickness data have also been corrected for elastic distortions of the testing apparatus and forcing blocks. (a) For a given loading rate, static friction and $\Delta\mu$ decrease with increasing hold time. Healing values decrease slightly with increasing velocity. (b) Compaction during unloading plotted for the same hold cycles shown in Figure 10a. Data do not show any significant dependence on hold time. (c) Layer compaction during zero-load holds is plotted as a function of time. Hold compaction increases with hold time. (d) Reload dilatancy is given for the same hold cycles shown above. The data show no significant dependence on hold time.

increasing η (e.g., the 100 s holds in Figure 13a). For each η we determine healing rate β with a least squares logarithmic fit. In order to compare data from the different studies we plot healing rate as a function of the coefficient of friction during holds (Figure 13b). The healing rates for bare granite are higher than our gouge results for all values of η. Both data sets show that healing rate decreases with decreasing η.

Our healing rates for gouge agree with results from previous studies [*Nakatani*, 1998; *Olsen et al.*, 1998]. However, both the absolute values of healing rate and the dependence on μ_{hold} differ

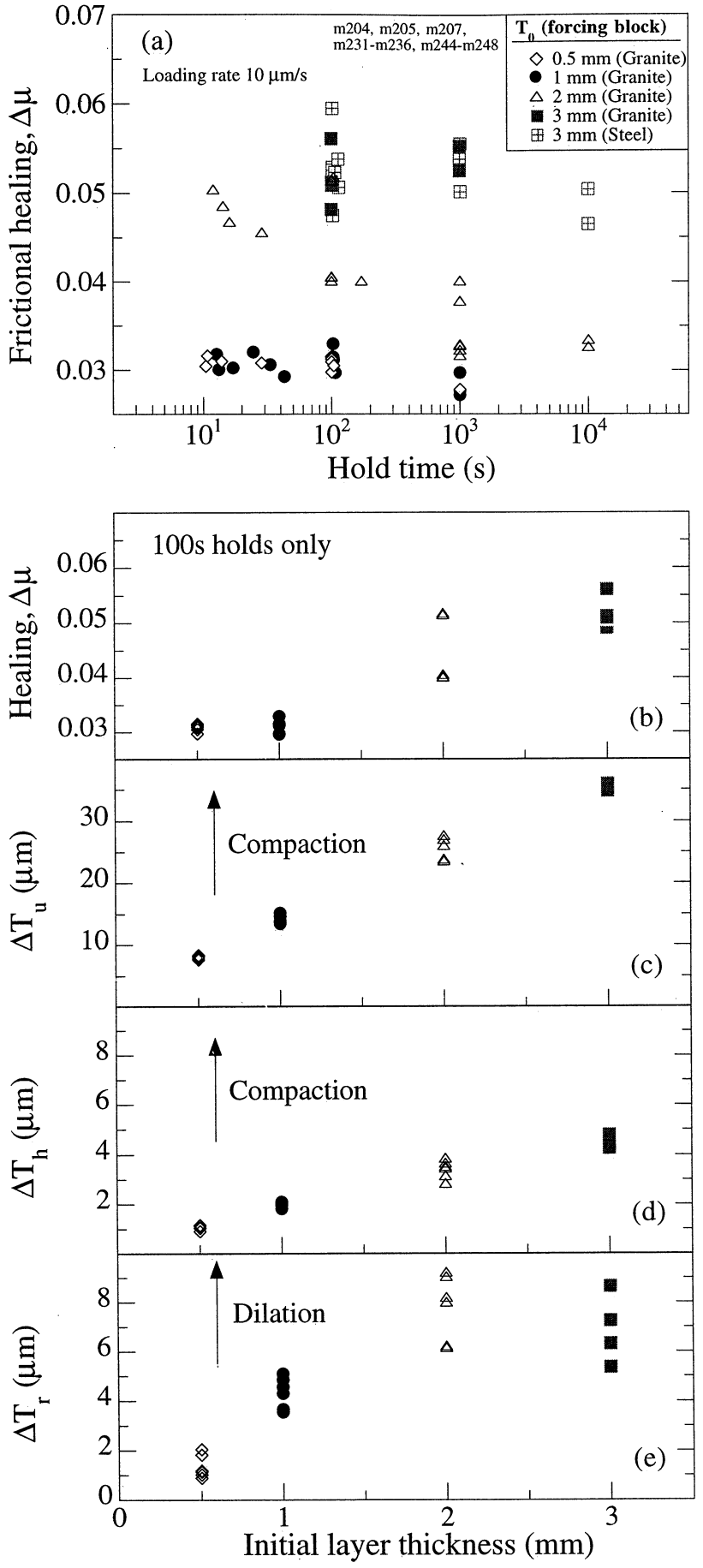
(a)
m204, m205, m207,
m231-m236, m244-m248
Loading rate 10 μm/s
T0 (forcing block)
0.5 mm (Granite)
1 mm (Granite)
2 mm (Granite)
3 mm (Granite)
3 mm (Steel)
Frictional healing, Δμ
Hold time (s)
100s holds only
Healing, Δμ
(b)
ΔTu (μm)
Compaction
(c)
ΔTh (μm)
Compaction
(d)
ΔTr (μm)
Dilation
(e)
Initial layer thickness (mm)

for tests on bare granite surfaces. This is another indication that despite the similarity of macroscopic frictional strength for gouge and bare surfaces (e.g., Byerlee's law) the microphysical processes of frictional shear differ significantly for the two cases.

4.3. Comparison to Predictions from Friction Laws

4.3.1. Existing rate and state constitutive laws. The rate- and state-dependent friction laws of *Dieterich* [1979] and *Ruina* [1983] describe friction in terms of loading rate and the evolving physical state of the sliding surface. Several variants of the laws have been suggested and applied to a wide range of materials and conditions [e.g., *Marone,* 1998b; *Géminard et al.*, 1999; *Baumberger et al.*, 1999; *Berthoud et al.*, 1999]. The laws each describe velocity and state dependence of friction with a relation:

$$\mu = \mu_0 + a\ln\left(\frac{V}{V_0}\right) + b\ln\left(\frac{V_0\theta}{D_c}\right). \quad (1)$$

Here μ_0 represents steady state friction for slip at a reference velocity V_0, V is sliding velocity, D_c is a critical slip distance, θ is a state variable, and a and b are scaling constants. The description of state evolution differs among the laws. The Dieterich evolution law

$$\frac{d\theta}{dt} = 1 - \left(\frac{V\theta}{D_c}\right), \quad (2)$$

permits state evolution for frictional surfaces held in true stationary contact (i.e., $V = 0$). However, the Ruina evolution law

$$\frac{d\theta}{dt} = -\frac{V\theta}{D_c}\ln\left(\frac{V\theta}{D_c}\right), \quad (3)$$

requires finite slip velocity for state evolution. We refer to (2) and (3) as the Dieterich and Ruina laws, respectively; they have also been referred to as the time (or slowness) and the slip evolution laws, respectively. In applying these laws to laboratory data, (1)-(3) are coupled to a relation for elastic interaction between the sample and loading apparatus: $d\mu/dt = k\,(V_0 - V)$, where V_0 is the initial loading velocity, and k is the apparatus stiffness divided by the normal stress ($k = 1.0\text{x}10^{-3}$ μm^{-1} for our apparatus at $\sigma_n = 25$ MPa).

4.3.2. Numerical simulations. *Karner and Marone* [1998] noted that the existing rate- and state-dependent friction laws did not adequately describe data for healing in simulated fault gouge (for $\eta < 1$) and healing on bare surfaces. Forward modeling of our reduced load tests (Figure 12) indicates that the laws predict significantly different healing levels as a function of η and different healing rates as a function of hold time. The Dieterich law predicts less healing as η increases for short hold times (10-100 s) and that healing is independent of η for longer hold times. The Ruina law predicts that healing is independent of η in the range 0-0.9 and increases above that. The Dieterich law predicts time-dependent strengthening in all cases, whereas the Ruina law predicts time-dependent strengthening only for $\eta > 0.9$ and no time-dependence for lower η.

It is apparent that neither friction law can predict the healing trends we observe experimentally when loading perturbations are far from steady state sliding conditions nor the trends for the bare surface tests of *Nakatani and Mochizuki* [1996]. This is perhaps not surprising, given that the laws were devised to describe small variations from steady frictional sliding for essentially bare contacting surfaces. For conditions near steady state the laws do an adequate job of describing granular friction; however, additional parameters are required to describe finite perturbations such as those imposed in our experiments. In particular, particle packing geometry and shear localization fabrics, in addition to porosity, must be accounted for in order to describe our observations. Although identifying and incorporating such terms in the laws is beyond the scope of this work, we discuss measurements and candidate physical properties below.

4.4. Healing and Compaction in Granular Gouge

Data from CSHS tests show that time-dependent strengthening is accompanied by positive compaction rates (Figure 3). This is consistent with the observed increase of healing and compaction as η decreases from 1 to 0 (e.g., Figure 7). Such a coupling is expected to the extent that the shear strength of a granular layer increases with layer density. However, for zero-load SHS tests we observe that time-dependent weakening is accompanied by positive compaction rates (Figure 10). This implies that time-dependent compaction during the wait periods of our healing tests occurs both within the zones of localized shear, which control frictional behavior, and in the relatively inactive regions outside these shear bands (e.g., see *Marone* [1998b] for a recent summary of shear localization in gouge). The same is likely to be true for the dilation we observe during reloading after a hold. Part of this dilatancy may occur outside the high strain rate shear bands. However, the relative proportions of porosity change within shear bands and inactive regions are likely to differ for dilatancy and time-dependent compaction. For dilatancy the requirement of shear-induced work and particle rearrangement limits participation by regions outside of shear bands. Compaction, on the other hand, can occur throughout the layer by stress relaxation and nearest neighbor rearrangements.

Figure 11. Data from gouge layers sheared at 10 μm/s investigating the effects of gouge layer thickness T_0. Data have been corrected for displacement and are referenced to 20 mm shear displacement. Layer thickness data have been corrected for elastic and volumetric distortions of the loading frame and forcing blocks, respectively. (a) Healing data as a function of initial layer thickness and hold time are shown; 2 mm and 3 mm layers display time-dependent weakening, while 0.5 mm and 1 mm layers show little time-dependent behavior. For a given hold time, healing levels are lower for thinner layers. (b) Healing data from all 100 s holds are plotted as a function of T_0. Healing increases directly with T_0. (c) Compaction during unloading is plotted and increases with T_0. (d) Amount of compaction during holds (ΔT_h) is plotted for the same 100 s hold cycles shown in Figures 11b and 11c. ΔT_h is greater for thicker gouge layers. (e) Dilatancy data are shown for the same hold cycles shown in Figures 11b-11d, showing increased dilatancy for greater T_0. For a given hold time, dilatancy is less than the net compaction that occurs prior to reloading.

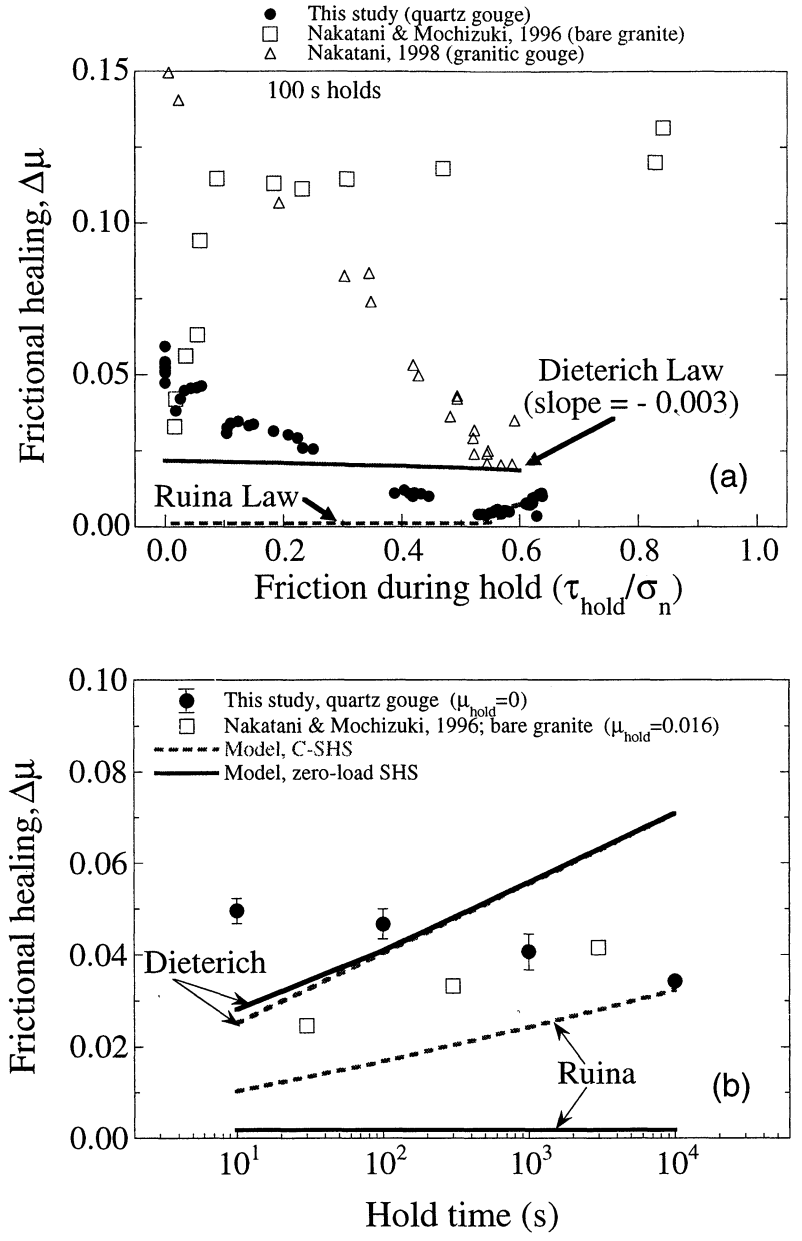

Figure 12. Our results are compared to gouge data from *Nakatani* [1998] and the bare surface friction data of *Nakatani and Mochizuki* [1996] together with healing predicted by the Dieterich and Ruina laws. We show *Nakatani*'s [1998] results from SHS cycles with hold times of 50 s and interpolate data from *Nakatani and Mochizuki* [1996] to 100 s hold times. For simulations, friction parameters were determined from velocity steps in our tests ($a = 0.0066$, $b = 0.0066$, and $D_c = 45$ μm). (a) We present a comparison between data and simulations, as a function of μ_{hold} (not η, as used previously). Our data from 100 s holds show lower healing levels and an inverse load dependence compared to data from bare granite surfaces. Dieterich law predicts healing levels similar to data and a slight inverse load dependence. Ruina law predicts the initial reduction in healing observed for μ_{hold} from 0.55 to 0.65 ($\eta \sim 0.9$-1). Below this level the Ruina law predicts no dependence on τ_{hold}, and healing levels are much lower than data. (b) Our results are compared to *Nakatani and Mochizuki*'s [1996] data ($\mu_{hold} = 0.016$) together with healing predictions for CSHS tests ($\eta = 1$) and zero-load tests ($\eta = 0$), respectively. We show the mean values of our zero-load data (bars indicate data range). Dieterich law predicts large positive healing rates, even for holds with true stationary contact. Ruina law predicts distinctly different healing rates depending on shear load. Neither the absolute value of $\Delta\mu$ nor the time dependence are well matched by model predictions.

Our data consistently show that compaction during hold cycles (unloading and holds) is greater than reload dilatancy (Figures 2, 4, 6-8, 10, and 11). This may be interpreted in terms of two end-member cases. (1) Hold cycles produce finite irrecoverable compaction due to grain fracturing and crushing. In this case, the particle size distribution should change continuously throughout our experiments. However, *Marone and Scholz* [1989] showed that the fractal dimension of simulated fault gouge remained constant for shear strains of 1.5-4, indicating that the gouge achieved a steady state particle size distribution. Recent work in

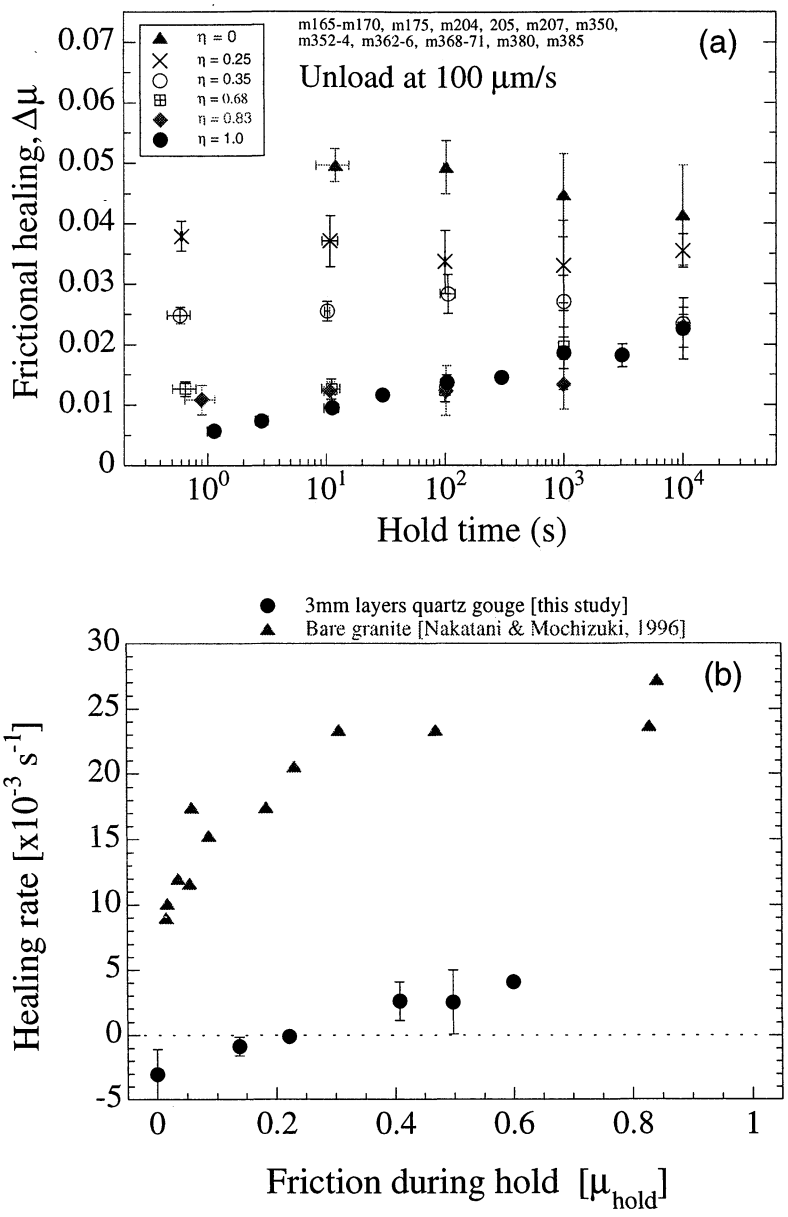

Figure 13. Healing data from tests at different levels of η are shown as a function of hold time. (a) We show mean healing values (symbols) with standard deviation (bars). Data show that Δμ systematically decreases with increasing η. Note the systematic transition in healing rates from time-dependent weakening (η = 0) to time-dependent strengthening (η = 1). (b) Healing rates β expressed as $\Delta\mu x10^{-3}$ per decade time (in seconds) were obtained from the tests plotted in Figure 13a, with bars indicating error (in terms of correlation coefficient, 1-*R*). Our results indicate that healing rate increases quasi-linearly with increasing η.

our laboratory extends this result to shear strains of 15 [*Mair and Marone,* 1999]. Thus, it seems unlikely that irrecoverable compaction is responsible for our observations. (2) Compaction and reload dilatancy measure deformation within different regions of the gouge, within shear bands and within intervening regions, as described above. We measure macroscopic changes in layer thickness, and thus we cannot independently resolve the spatial distribution of layer density or its influence on frictional strength. However, this interpretation is supported by intermediate η data, which indicates a complicated relationship between fault healing and gouge deformation.

In Figure 14 we compare data from experiments with η = 1.0 and 0.83. For η = 0.83, healing is approximately constant for shorter hold times (<100 s) but increases for longer hold times. This implies that time-dependent healing processes are aided by stress-induced mechanisms. Compaction data from these tests are plotted in Figure 14b. As expected, unloading compaction (open symbols) is constant for all hold times. Compaction during holds (solid symbols) increases with hold time, and the compaction rate is independent of η. These results, which were reproduced in repeat experiments, indicate that a significant fraction of the time-dependent consolidation signal is due to densification in regions outside of the active shear bands. As the shear bands are expected to play a dominant role in setting frictional strength and constitutive characteristics during shear, the observations of Figure 14 explain why we observe time-

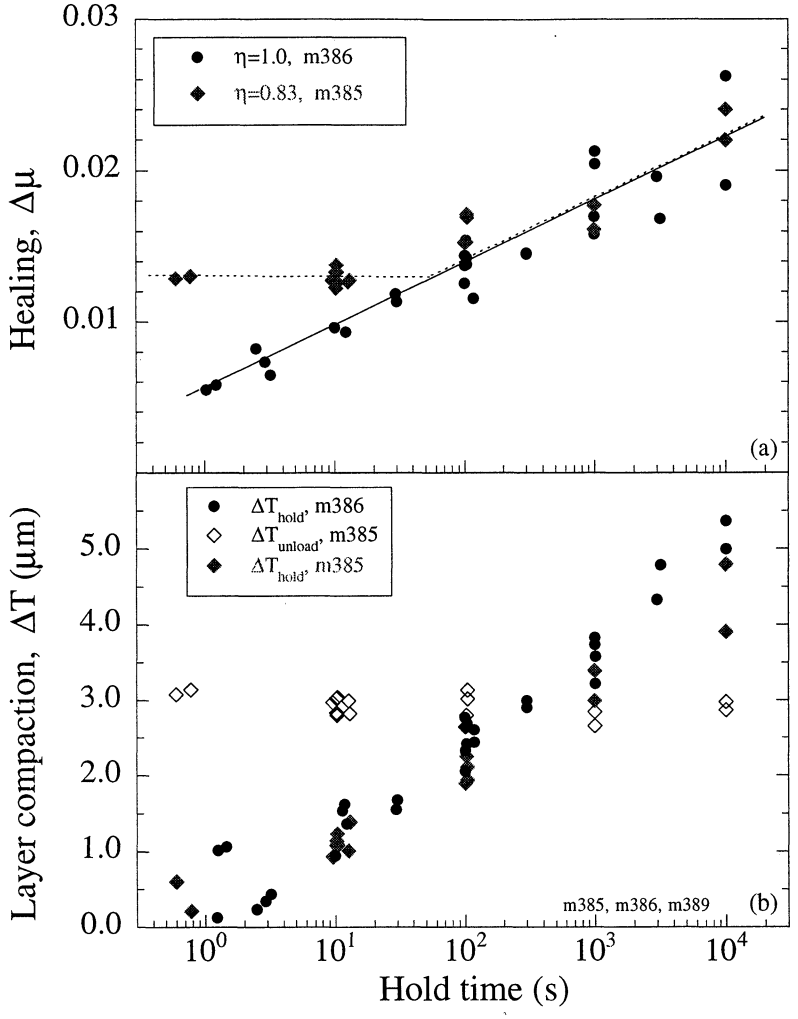

Figure 14. Comparison of results from a reduced load SHS test ("m385" where $\eta = 0.83$) to data from CSHS tests (from Figure 3). (a) Our reduced-load SHS data show little change in healing levels for short hold times (<100 s) yet increasing healing for longer hold times (>100 s). Thus, for the $\eta = 0.83$ tests a transition in healing rate occurs at hold times of ~100 s. (b) Compaction data for the same tests in Figure 14a show that time-dependent layer compaction during holds for the CSHS and "m385" are similar. However, the difference between the experiments is the unloading that occurs for "m385", for which we observe no time dependence.

dependent weakening together with bulk densification for low η (e.g., Figure 13). When shear stress is reduced, a critical wait time is necessary before time-dependent processes become significant relative to stress-induced healing. We expect that this critical wait time scales inversely with η, which explains why our healing rates are zero or negative for η less than ~0.68 (note that $\eta = 0.68$ corresponds to $\mu_{hold} = 0.41$ in Figure 13b).

Compaction and dilation are key aspects of gouge deformation, and it is important to understand their role in frictional healing. Previous works have shown that shear localization and stress inhomogenities play a significant role in the mechanics of granular materials [e.g., *Marone*, 1998b]. Therefore we present further analysis of porosity changes below after introducing these topics.

4.5. Micromechanical Model of Healing in Granular Gouge

Studies of granular deformation indicate that the state of the system cannot always be adequately described by the macroscopically measured stress and strain [*Sammis and Steacy*, 1994; *Williams and Rege*, 1997], and that factors such as porosity, consolidation, particle shape, grain packing, particle size distribution, and shear fabric must be considered [*Chester and Logan*, 1989; *Biegel et al.*, 1989; *Marone and Kilgore*, 1993; *Beeler et al.*, 1996; *Jaeger et al.*, 1996; *Oda*, 1997; *Williams and Rege*, 1997; *Cates et al.*, 1998; *Morgan*, 1999; *Morgan and Boettcher*, 1999; *Géminard et al.*, 1999; *Losert et al.*, 2000]. We concentrate here on correlations between healing and gouge layer thickness variations, the latter being indicative of porosity evolution, consolidation state, and layer density.

Our observation of time-dependent frictional weakening in a granular system is novel and interesting on its own. We observe bulk layer densification together with weakening. These observations are surprising in the context of healing models based solely on contact area [e.g., *Dieterich*, 1972]. However, the data are expected from models where stress chains play a role in granular deformation [e.g., *Sammis et al.*, 1987; *Sammis and Steacy*, 1994; *Oda*, 1997]. In this model, optimally oriented particulate chains act to support a sizable portion of the applied load (the "ligands" of *Sammis et al.* [1987]) and the mechanical properties and population of the chains determine the

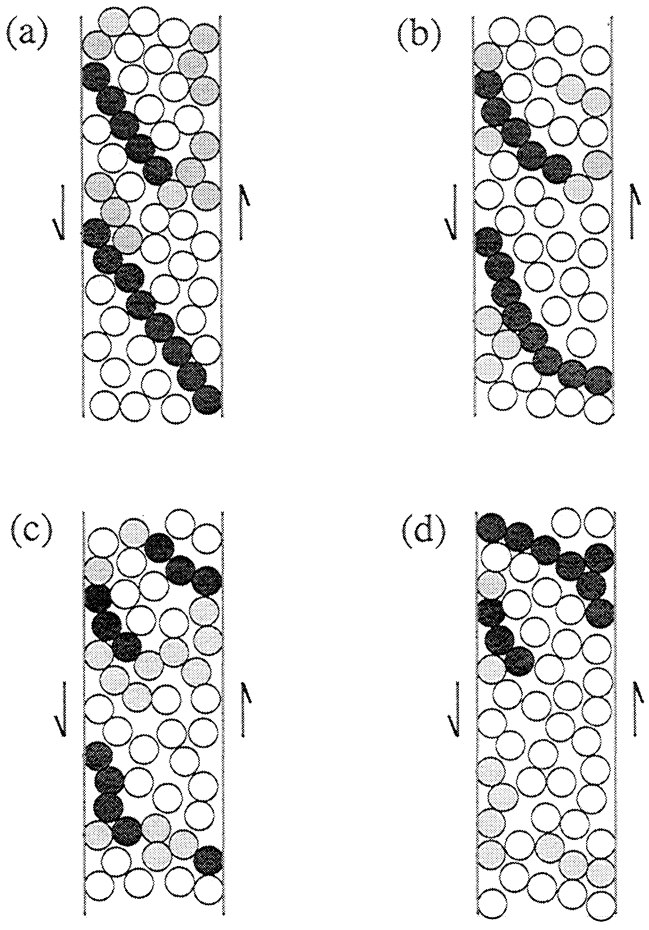

Figure 15. Schematic illustration of force chains (dark shading) and jamming within deforming gouge layers. Grains responsible for significant resistance to layer deformation (i.e., jamming force chains) are darker. (a-d) Force chain evolution is shown for consecutive intervals of shear. Our observations of slip reversal for low τ_{hold} (Figure 6d) are consistent with elastic unloading of force chains. We interpret time-dependent weakening (Figure 9) as the result of interparticle creep and disruption of force chains.

macroscopic deformation behavior (Figure 15). For example, the growth of stress chains may facilitate a blockage of granular flow (jamming), which may collapse with subsequent perturbations of the system [*Ball and Melrose*, 1995; *Farr et al.*, 1997; *Cates et al.*, 1998; *Liu and Nagel*, 1998].

4.5.1 Stress chains and shear deformation. We propose a model in which the frictional strength of sheared granular layers is the product of two factors: (1) geometric strength of granular stress chains and (2) time-dependent strength of particle contacts. For our experiments, stress chains form during shearing, and significant interparticle shear stresses persist within chains even after unloading. Recall that our loading conditions are constant normal stress and a varying shear stress. For holds at high macroscopic shear stress and η near unity, interparticle stresses aid time-dependent processes, and the frictional strength of layers increases via contact junction growth and consolidation within shear bands. In this case, mean stress within layers is sufficient to inhibit significant slip between chain particles, and thus the geometric strength of stress chains is preserved while contact junction strength increases. When subject to shear, these layers are strong and frictional yield strength increases with time. At low macroscopic shear stress and η near zero, mean stress is insufficient to inhibit interparticle slip within chains. Large interparticle slip may erase contact junction growth if existing contacts are, on average, replaced rather than enlarged. In addition, large interparticle slip will degrade the geometric strength of stress chains, causing disruption and weakening. In effect, for the unstressed aging case we envision a weakening mechanism based on time-dependent unjamming of sheared granular layers. Our experiments indicate that the critical shear stress for the transition from time-dependent weakening to strengthening is roughly 30% of the normal stress (Figure 13b).

Two other aspects of our data can now be understood. First, although holds at $\eta = 0$ result in time-dependent weakening, the absolute value of static yield strength is largest in this case. In fact, our data show that static yield strength increases systematically as η approaches zero (Figure 7). Furthermore, our layer compaction data indicate that the η-dependent restrengthening occurs in the same region of the gouge that produces the time-dependent weakening for η near zero. This implies that restrengthening processes must operate only during unloading before unjamming and time-dependent weakening occurs during holds. Thus we propose that peak static yield strength is a measure of the geometric strength of stress chains and that stress chains strengthen during unloading. The geometric strength of stress chains increases during unloading due to consolidation and grain rearrangement. This increase in strength is not lost immediately upon reloading because interparticle slip within chains is inhibited by increasing mean stress, consistent with our observation that reload dilatancy is systematically smaller than unload compaction (Figure 7). Instead, peak strength is high, and finite shearing is required to erase strengthening associated with unloading (Figure 8).

The second aspect involves the time dependence of weakening for low η cases. We propose that the reason weakening exhibits a logarithmic time dependence (e.g., Figures 9 and 13) is that interparticle slip obeys a rate-state friction-type relation. Particle rearrangement and destruction of stress chains is the result of relaxation of residual stresses, which is governed by frictional slip. Thus the observation of time-dependent weakening is consistent with adhesive friction theory and contact mechanics as long as the role of stress chains in granular material is recognized.

4.5.2. Particle-based numerical simulations. Further insight into the deformation of granular media may be obtained from experiments designed to directly view the deformation features or from numerical simulations that investigate shear deformation within granular media [e.g., *Morgan*, 1999; *Morgan and Boettcher*, 1999]. The numerical simulations of shear in simulated fault gouge [e.g., *Morgan and Boettcher*, 1999] suggest that regions within the layers can episodically lock up and become more resistant to continued deformation. Chains of load-bearing particles develop in front of the locked regions and are approximately collinear with the orientation of the maximum compressive stress. With continued macroscopic shear, these chains rotate with the sense of shear and eventually collapse. Chain collapse correlates with increased granular flow, consistent with unjamming of the system and can be subsequently followed by jamming in other regions of the layer.

5. Summary

In order to broaden the range of physical conditions studied for the mechanical behavior of faults and to test the existing rate-

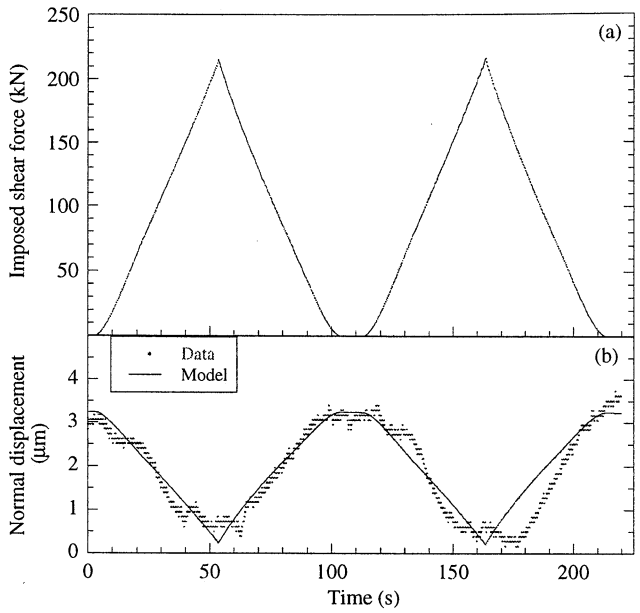

Figure A1. Calibration data to investigate Poisson distortion of the forcing blocks. A rectangular block of steel was subjected to stresses consistent with our experiments (constant "normal" stress of 25 MPa and varying "shear" force). (a) The imposed "shear" force was cycled from zero to a peak value that exceeded 200 kN. (b) The measured piston displacement required to maintain constant "normal" stress is shown for the loading cycles plotted in Figure A1a. Also plotted is the predicted displacement using the plane stress approximation (equation (A1)). The calculated displacement arising from the imposed loading variations matches the data.

and state-dependent friction laws we have performed slide-hold-slide (SHS) experiments on simulated fault gouge in a double-direct shear testing apparatus. We have investigated the effects of shear load, hold time, loading rate, and initial layer thickness on frictional restrengthening (healing). Our data show systematic trends as a function of these variables. Healing and layer compaction increase with decreasing shear load for holds. From tests where $\eta = 0$ our data consistently show time-dependent weakening. Healing decreases as a function of decreasing initial layer thickness.

Numerical simulations using the rate- and state-dependent friction laws indicate that neither the Dieterich nor Ruina laws are capable of describing our data over the full range of conditions studied. We present a micromechanical model based on load-bearing particulate chains within the gouge and time-dependent unjamming. The existence of a given stress chain may be short-lived, but we propose that these chains are both destroyed and created during active shear deformation of granular gouge. Steady state sliding would represent an equilibrium between the generation and collapse of stress chains. Our data show that time-dependent shear deformation at grain contacts leads to time-dependent destruction of stress chains.

Appendix A: Corrections to Layer Thickness Data

A first-order observation from our experiments is that layers thin considerably with progressive shear (Figure 4b). This is consistent with previous studies using the double-direct shear configuration, where the slip-dependent evolution of layer thickness has been attributed to geometric constraints [e.g., *Scott et al.*, 1994]. For clarity and to assist with analysis of our results, we fit and remove a linear trend from the data to account for geometric thinning. As per the analysis of *Scott et al.* [1994], this linear trend corresponds to extrusion of gouge with progressive shear. Thus, by removing this geometric thinning from our data we can better investigate the relationship between healing and gouge densification for hold cycles.

We must also address another aspect of reduced-load SHS tests, whereby sample forcing blocks experience Poisson-like distortions owing to the large variations in applied shear load. Ideally, layer thickness would be measured from one stationary side block to the center block. However, in practice we must fix the displacement transducers to the stationary side blocks. This limitation arises because of the motion of the center forcing block during shear. Thus to remove the effects of the Poisson distortion, we correct the layer thickness data from all our reduced-load tests using a plane stress approximation:

$$\varepsilon_2 = \frac{1}{E}(\sigma_2 - \upsilon\sigma_1), \qquad \text{(A1)}$$

where σ and ε are the applied tractions and strains perpendicular to each loaded surface of the center block. The subscripts 1 and 2 refer to the loading axes of the shear and normal stresses (which are essentially σ_1 and σ_2 in (A1), respectively), and ν and E are the Poisson ratio and Young's modulus for the forcing block material (described previously in section 2.1). The corrections incorporate measured thickness and surface areas of the center forcing block. We have performed calibrations on the testing apparatus and forcing block materials, and these indicate that the plane stress approximation is sufficient for correcting the layer thickness measurements [*Karner*, 1999] (see Figure A1). For complete removal of shear load, this correction to the layer thickness data is 1-5 μm (depending on forcing block dimensions and material).

Acknowledgments. We thank Einat Aharonov, Paul Segall, and Teruo Yamashita for their thought-provoking and thorough reviews of this manuscript. We have enjoyed the many discussions about this work that we have had with Kevin Frye, Karen Mair, Eliza Richardson, and David Sparks. We also thank Nathan Kuhle and Steve Lenz for their careful editorial reviews of this paper. This research was supported by NSF Grants EAR-9627895 and EAR- 9805327 and by USGS Grant 99HQGR0003.

References

Ball, R.C., and J.R. Melrose, Lubrication breakdown in hydrodynamic simulations of concentrated colloids, *Adv. Colloid Interface Sci.*, *59*, 19-31, 1995.

Baumberger, T., P. Berthoud, and C. Caroli, Physical analysis of the state- and rate-dependent friction law: II. Dynamic friction, *Phys. Rev. B*, *60*, 3928-3939, 1999.

Beeler, N.M., T.E. Tullis, and J.D. Weeks, The roles of time and displacement in the evolution effect in rock friction, *Geophys. Res. Lett.*, *21*, 1987-1990, 1994.

Beeler, N.M., T.E. Tullis, and J.D. Weeks, Frictional behavior of large displacement experimental faults, *J. Geophys. Res.*, *101*, 8697-8715, 1996.

Berthoud, P., T. Baumberger, C. G'Sell, and J.-M. Hiver, Physical analysis of the state- and rate-dependent friction law: Static friction, *Phys. Rev. B*, *59*, 14,313-14,327, 1999.

Biegel, R.L., C.S. Sammis, and J.H. Dieterich, The frictional properties of a simulated gouge having a fractal particle distribution, *J. Struct. Geol.*, *11*, 827-846, 1989.

Blanpied, M.L., D.A. Lockner, and J.D. Byerlee, Fault stability inferred from granite sliding experiments at hydrothermal conditions, *Geophys. Res. Lett.*, *18*, 609-612, 1991.

Byerlee, J.D., Frictional characteristics of granite under high confining pressure, *J. Geophys. Res.*, 72, 3639-3648, 1967.

Cates, M.E., J.P. Wittmer, J-P Bouchaud, and P. Claudin, Jamming, force chains, and fragile matter, *Phys. Rev. Lett.*, *81*, 1841-1844, 1998.

Chester, F.M., and N.G. Higgs, Multimechanism friction constitutive model for ultrafine quartz gouge at hypocentral conditions, *J. Geophys. Res.*, *97*, 1857-1870, 1992.

Chester, F.M., and J.M. Logan, Composite planar fabric of gouge from the Punchbowl Fault, California, *J. Struct. Geol.*, *9*, 621-634, 1989.

Dieterich, J.H., Time-dependent friction in rocks, *J. Geophys. Res.*, *77*, 3690-3697, 1972.

Dieterich, J.H., Time-dependent friction and the mechanics of stick-slip, *Pure Appl. Geophys.*, *116*, 790-805, 1978.

Dieterich, J.H., Modeling of rock friction: 1. Experimental results and constitutive equations, *J. Geophys. Res.*, *84*, 2161-2168, 1979.

Farr, R.S., J.R. Melrose, and R.C Ball, Kinetic theory in hard-sphere startup flows, *Phys. Rev. E*, *55*, 7203-7211, 1997.

Fredrich, J.T., and B. Evans, Strength recovery along simulated faults by solution transfer processes, *Proceedings of the 33rd National Rock Mechanics Symposium*, edited by W. Wawersik, pp. 121-130, A.A. Balkema, Brookfield, Vt, 1992.

Géminard, J.-C., W. Losert, and J.P. Gollub, Frictional mechanics of wet granular material, *Phys. Rev. E*, *59*, 5881-5890, 1999.

Heslot, F., T. Baumberger, B. Perrin, B. Caroli, and C. Caroli, Creep, stick-slip, and dry-friction dynamics: Experiments and a heuristic model, *Phys. Rev. E*, *49*, 4973-4988, 1994.

Jaeger, H.M., S.R. Nagel, and R.P. Behringer, The physics of granular materials, *Phys. Today*, *49*(4), 32-38, 1996.

Karner, S.L., Laboratory analysis of restrengthening on simulated faults, Ph.D. thesis, Mass. Inst. of Technol., Cambridge, Massachusetts, 1999.

Karner, S.L., and C. Marone, The effect of shear load on frictional healing in simulated fault gouge, *Geophys. Res. Lett.*, *25*, 4561-4564, 1998.

Karner, S.L., C. Marone, and B. Evans, Laboratory study of fault healing and lithification in simulated fault gouge under hydrothermal conditions, *Tectonophysics*, *277*, 41-55, 1997.

Linker, M.F., and J.H. Dieterich, Effects of variable normal stress on rock friction: Observations and constitutive equations, *J. Geophys. Res.*, *97*, 4923-4940, 1992.

Liu, A.J., and S.R. Nagel, Jamming is not just cool any more, *Nature*, *396*, 21-22, 1998.

Lockner, D.A., R. Summers, and , J.D. Byerlee, Effects of sliding rate and temperature on frictional strength of granite, *Pure Appl. Geophys.*, *124*, 445-469, 1986.

Losert, W., J.-C. Géminard, S. Nasuno, and J.P. Gollub, Mechanisms for slow strengthening in granular materials, *Phys. Rev. E*, *61*, 4060-4068, 2000.

Mair, K., and C. Marone, Friction of simulated fault gouge for a wide range of velocities and normal stresses, *J. Geophys. Res.*, *104*, 28899-28914, 1999.

Marone, C., The effect of loading rate on static friction and the rate of fault healing during the earthquake cycle, *Nature*, *391*, 69-72, 1998a.

Marone, C., Laboratory derived friction laws and their application to seismic faulting, *Annu. Rev. Earth Planet. Sci.*, *26*, 643-696, 1998b.

Marone, C., and B. Kilgore, Scaling of the critical slip distance for seismic faulting with shear strain in fault zones, *Nature*, *362*, 618-621, 1993.

Marone, C., and C.H. Scholz, Particle-size distribution and microstructures within simulated fault gouge, *J. Struct. Geol.*, *11*, 799-814, 1989.

Marone, C., C.B. Raleigh, and C.H. Scholz, Frictional behavior and constitutive modeling of simulated fault gouge, *J. Geophys. Res.*, *95*, 7007-7025, 1990.

Morgan, J.K., Numerical simulations of granular shear zones using the distinct element method, 2: Effects of particle size distribution and interparticle friction on mechanical behavior, *J. Geophys. Res.*, *104*, 2721-2732, 1999.

Morgan, J.K., and M.S. Boettcher, Numerical simulations of granular shear zones using the distinct element method, 1: Shear zone kinematics and the micromechanics of localization, *J. Geophys. Res.*, *104*, 2703-2719, 1999.

Nakatani, M., A new mechanism of slip-weakening and strength recovery of friction associated with the mechanical consolidation of gouge, *J. Geophys. Res.*, *103*, 27239-27256, 1998.

Nakatani, M., and H. Mochizuki, Effects of shear stress applied to surface in stationary contact on rock friction, *Geophys. Res. Lett.*, *23*, 869-872, 1996.

Nasuno, S., A. Kudrolli, and J.P. Gollub, Friction in granular layers: Hysteresis and precursors, *Phys. Rev. Lett.*, 79, 949-952, 1997.

Nasuno, S., A. Kudrolli, A. Bak, and J.P. Gollub, Time-resolved studies of stick-slip friction in sheared granular layers, *Phys. Rev. E*, *58*, 2161-2171, 1998.

Oda, M., A micro-deformation model for dilatancy of granular materials, *Mechanics of Deformation and Flow of Particulate Materials*, edited by C.S. Chang et al., pp. 24-37, Am. Soc. Civ. Eng., New York, 1997.

Olsen, M.P., C.H. Scholz, and A. Léger, Healing and sealing of a simulated fault gouge under hydrothermal conditions: Implications for fault healing, *J. Geophys. Res.*, *103*, 7421-7430, 1998.

Perrin, G., J.R. Rice, and G. Zheng, Self-healing slip pulse on a frictional surface, *J. Mech. Phys. Solids*, *43*, 1461-1495, 1995.

Richardson, E., and C. Marone, Effects of normal stress vibrations on frictional healing, *J. Geophys. Res.*, *104*, 28859-28878, 1999.

Ruina, A., Slip instability and state variable friction laws, *J. Geophys. Res.*, 88, 10,359-10,370, 1983.

Sammis, C.G., and S.J. Steacy, The micromechanics of friction in a granular layer, *Pure Appl. Geophys.*, *142*, 777-794, 1994.

Sammis, C., G. King, and R. Biegel, The kinematics of gouge deformation, *Pure Appl. Geophys.*, *125*, 777-812, 1987.

Scholz, C.H., Wear and gouge formation in brittle faulting, *Geology*, *15*, 493-495, 1987.

Scott, D.R., C. Marone, and C.G. Sammis, The apparent friction of granular fault gouge in sheared layers, *J. Geophys. Res.*, *99*, 7231-7246, 1994.

Segall, P., and J.R. Rice, Dilatancy, compaction, and slip instability of a fluid infiltrated fault, *J. Geophys. Res.*, *100*, 22,155-22,171, 1995.

Sleep, N.H., Ductile creep, compaction, and rate and state dependent friction within major fault zones, *J. Geophys. Res.*, *100*, 13,065-13,080, 1995.

Williams, J., and N. Rege, Granular vortices and shear band formation, *Mechanics of Deformation and Flow of Particulate Materials*, edited by C.S. Chang et al., pp. 62-76, Am. Soc. Civ. Eng., New York, 1997.

S.L. Karner, Department of Geology and Geophysics, Center for Tectonophysics, Texas A&M University, College Station, TX, 77843-3113, USA. (Email: karner@geo.tamu.edu)

C. Marone, Department of Geosciences, Pennsylvania State University, University Park, PA, 16802, USA. (Email: cjm38@psu.edu)

(Received August 18, 2000; revised April 23, 2001;
accepted June 4, 2001)